Research Article

Peiyu You, Hui Chen, Mingjie Li and Ye Wu*

A simulative study on the effect of friction coefficient and angle on failure behaviors of GLARE subjected to low-velocity impact

https://doi.org/10.1515/secm-2022-0194
received November 14, 2022; accepted March 13, 2023

Abstract: The aim of this paper is to study the effect of friction coefficient and impact angle on the failure behaviors of glass fiber reinforced aluminum laminates (GLARE) under the low-velocity impact (LVI) loading. A methodology is developed in commercial software ABAQUS/Explicit, and its accuracy is verified based on the results of comparison between simulation and experiment. In the simulation, Johnson–Cook flow stress model and surface-based cohesive behavior are carried out to simulate the damage evolution of aluminum alloy layers and delamination at the interface. Further, both the dynamic response history and damage mechanism characterization of these hybrid laminates are presented and compared carefully. Additionally, due to the advantage of simulation, it is accurate and easy to discuss on the evolution of the damage contour consisting of the damage degree of composite and metal layers as well as the interface between them. Finally, the influence rules of friction coefficient and angle on the failure behaviors of GLARE under LVI are drawn clearly.

Keywords: GLARE, low-velocity impact, FE simulation, damage evolution

1 Introduction

Composites offer many advantages compared to metallic alloys, especially where high strength and stiffness-to-weight ratio are concerned. And, it is used in various fields ranging from aviation and space [1] to civil engineering [2] and marine [3,4] applications due to their inherently high specific mechanical properties as well as low weight.

In recent years, numerous tests have been carried out to obtain the effects of impact on fiber reinforced polymer (FRP) and fiber metal laminates (FML) laminates [5,6]. To enhance the impact resistance, metal wire nets were inserted into glass FRP laminates [7–9]. The hybrid materials consisting of more than two types of fiber fabric may contain the advantages of each ingredient, thus improving the impact resistance. Yang et al. [10] investigated the impact response of hybrid FRPs, and the results showed that the impact-resistance performance of carbon FRPs could be enhanced by the addition of glass fiber layers. Song et al. [11] and Gu et al. [12] experimentally investigated the low-velocity impact (LVI) responses of hybrid FRP composites. It was found that a hybrid composite would help minimize the risk of damage and enable rapid prototyping toward composite designs with optimal impact-resistant properties. Researchers also investigated the low-velocity properties of nanofiller-modified composites. For example, Song et al. [11] studied the impact behaviors of CNT-reinforced functionally graded composite plates. The LVI performance of nanoclay-GF/epoxy composites was studied by Rafiq et al. [13]. It was found that the addition of nanomaterials could improve the peak load and stiffness of the material during the impact event.

Competing materials like advanced aluminum alloys and FRP increase the cost effectiveness of the structure. These materials still have their advantages and disadvantages, like the poor fatigue strength of the aluminum alloys and the poor impact and residual strength properties of FRP. However, impact damage and fatigue failure are important types of failure for composite structures. To balance fatigue and impact performance, the idea of using two materials to fabricate a hybrid composite structural material to combine the advantages of both materials was presented by the Delft University of Technology [14].

* **Corresponding author: Ye Wu,** School of Civil and Architecture Engineering, Nanchang Institute of Technology, No. 289, Tianxiang Road, Nanchang, Jiangxi Province, China, e-mail: 0224141@163.com
Peiyu You, Mingjie Li: School of Civil and Architecture Engineering, Nanchang Institute of Technology, No. 289, Tianxiang Road, Nanchang, Jiangxi Province, China
Hui Chen: School of Hydraulic and Ecological Engineering, Nanchang Institute of Technology, Nanchang, China

The FMLs are materials characterized by the bonding of a conventional FRP with metal layers. Due to the high ductility of the metal layer, FML laminates are characterized by better performance to LVI than regular FRP composites [15]. However, in addition to the types of damages in composite materials, i.e., fiber cracks, and matrix cracks which is similar to the rock [16–19], the complexity of FML structure easily leads to delamination at the metal–composite interface. Li et al. [20] investigated the dynamic response and damage mechanism characterization of GLARE under single and repeated LVI. For GLARE, the interface delamination between composite and metal layer is one of the main failure modes [21]. Thus, there are lots of studies regarding the delamination behavior under LVI load, including experimental [22,23] and numerical studies by C-scan and cohesive zone model [24,25], respectively. The results indicated that crack growth at the weak bonding interface lead this type of laminate to have poor interlaminate shear strength.

As far as the authors acknowledge, there is only little literature available that explains the effects of the friction coefficient between impactor and FML and impact angle in LVI events on the failure modes and mechanisms. Moreover, in the LVI testing of ASTM D 7136M, there is no option to investigate the parameter of impact angle. Besides, the parameter of friction coefficient is hard to control in the experiments. Fortunately, in the FEM, both of them could be easily and accurately changed.

In this study, a methodology is developed in commercial software ABAQUS/Explicit to study the effect of friction coefficient and angle on the failure behaviors of GLARE under LVI loading. During the LVI events, based on the damage evolution consisting of the aluminum alloy layers, fiber reinforced plastic (FRP) layers and the interface between them. The influence rules of friction coefficient and angle on the failure behaviors of GLARE are drawn deeply and clearly.

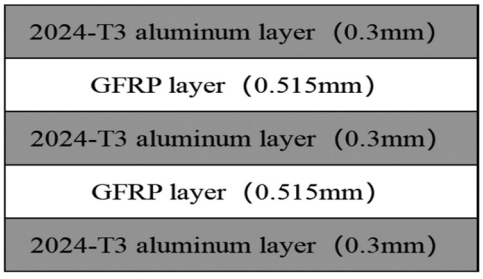

Figure 1: The configuration of GLARE (3/2).

2 Materials and methods of the LVI test

In the experiments by Seyed Yaghoubi et al. [22], all GLARE panels consist of 2024-T3 aluminum alloy of 0.305 mm/layer and S2-glass-epoxy layer of 0.515 mm/layer. Each S2-glass-epoxy layer has a layup orientation of [0°/90°] s. Figure 1 shows the configuration of GLARE (3/2). GLARE 5 panels with various thicknesses were cut into square specimens with dimensions of 101.6 mm × 101.6 mm.

In the LVI tests shown in Figure 2, the panels are clamped via two steel plates with a hole of 76.2 mm diameter. During the impact process, the contact force and displacement history of the impactor with a hemispherical top of 16 mm diameter and 12.9 kg mass are recorded. Then, the C-scan device is employed to inspect the internal damage degree including interface delamination after the LVI loading.

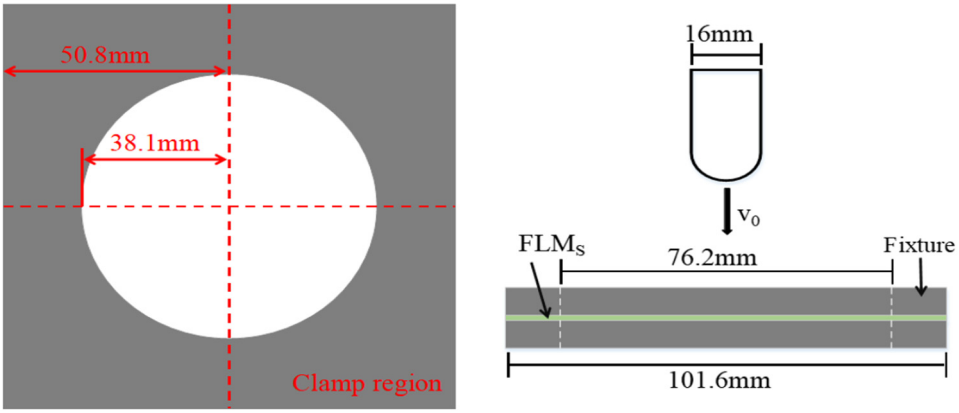

Figure 2: The set-up of LVI experiment.

3 Building up the finite element model (FEM) for the GLARE subjected LVI loading

As mentioned above, in addition to FRP and aluminum alloy layers, the GLARE is sensitive to the interlaminar delamination caused by the loading, such as shear, LVI, and so on, hence, the FEM model is consisted of these two types of layers and interlaminar damage.

3.1 FEM and element type

The commercial software ABAQUS/Explicit is employed to develop the methodology for the damage assessment of GLARE subjected to LVI loading. In the simulation, the impactor is defined as a semicircular discrete rigid body using R3D4 elements with 16 mm diameter and 12.9 kg mass. To obtain accurate results, the seeds are scattered with higher density around the impact region. The element type of FRP and aluminum alloy layers is C3D8R. To reduce the computational time by decreasing the number of elements, the outer areas are meshed with a coarse seed size. In our simulation, the user material subroutine VUMAT, Johnson–Cook flow stress model, and surface-based cohesive behavior are combined to evaluate the GLARE 5's failure involved in the FRP layers, aluminum alloy layers, and the interlaminar delamination between two types of layers, respectively.

3.2 Hashin damage criterion for FRP

Hashin damage initiation criterion [26], one of the most widely used damage criterions for FRP, is employed to develop the user material subroutine VUMAT, in which the GFRP failure is studied properly based on the following criteria with the properties listed in Table 1.

Delamination, $\sigma_{33} > 0$

$$\left(\frac{\sigma_{33}}{Z_t}\right)^2 + \left(\frac{\tau_{31}}{S_{31}}\right)^2 + \left(\frac{\tau_{23}}{S_{23}}\right)^2 \geq 1. \tag{1}$$

Delamination, $\sigma_{33} < 0$

$$\left(\frac{\tau_{31}}{S_{31}}\right)^2 + \left(\frac{\tau_{23}}{S_{23}}\right)^2 \geq 1. \tag{2}$$

Tensile damage of the matrix, $\sigma_{22} + \sigma_{33} > 0$

Table 1: Material properties of UD S2 glass/FM 94 epoxy prepreg layers [22]

Property	Value	Property	Value
E_{11} (GPa)	54	X_T (MPa)	1,900
E_{22} (GPa)	9.4	X_C (MPa)	520
E_{33} (GPa)	9.4	Y_T (MPa)	57
μ_{12}	0.0575	Y_C (MPa)	285
μ_{13}	0.0575	Z_T (MPa)	57
μ_{23}	0.33	Z_C (MPa)	285
G_{12} (GPa)	5.6	S_{12} (GPa)	76
G_{13} (GPa)	5.6	S_{13} (GPa)	76
G_{23} (GPa)	5.6	S_{23} (GPa)	76

$$\left(\frac{\sigma_{22} + \sigma_{33}}{Y_T}\right)^2 + \frac{1}{S_{23}^2}(\tau_{23}^2 - \sigma_{22}\sigma_{33}) + \left(\frac{\tau_{12}}{S_{12}}\right)^2 + \left(\frac{\tau_{31}}{S_{31}}\right)^2 \geq 1. \tag{3}$$

Compressive damage of the matrix, $\sigma_{22} + \sigma_{33} > 0$

$$\frac{1}{Y_C}\left[\left(\frac{T_C}{2S_{12}}\right)^2 - 1\right](\sigma_{22} + \sigma_{33}) + \left(\frac{\sigma_{22} + \sigma_{33}}{2S_{12}}\right)^2 + \frac{1}{S_{23}^2}(\tau_{23}^2 - \sigma_{22}\sigma_{33}) + \left(\frac{\tau_{12}}{S_{12}}\right)^2 + \left(\frac{\tau_{31}}{S_{31}}\right)^2 \geq 1. \tag{4}$$

Tensile damage of the fibers, $\sigma_{11} \geq 0$

$$\left(\frac{\sigma_{11}}{X_T}\right)^2 + \left(\frac{\tau_{12}}{S_{12}}\right)^2 + \left(\frac{\tau_{13}}{S_{13}}\right)^2 \geq 1. \tag{5}$$

Compressive damage of the fibers, $\sigma_{11} \leq 0$

$$\left(\frac{\sigma_{11}}{X_C}\right)^2 \geq 1. \tag{6}$$

The discrete degradation model lowers the stiffness of composite materials by reducing the elasticity modulus by multiplying it with a coefficient less than 1. When the material reaches one damage initiation criteria in all kinds of damage modes the material stiffness starts declining in a way of the coefficient reduction of 0.1 in this study.

Table 2: Material properties of aluminum alloy

Property	Value
Elastic parameters	E = 72 GPa, μ = 0.33
Yield surface parameters	A = 359 MPa, B = 455 MPa, C = 0.15, m = 1, n = 0.34
Failure parameters	d_1 = 0.13, d_2 = 0.13, d_3 = 1.5, d_4 = 0.011
Fracture energy	G_{IC} = 8 kJ/m^2

Table 3: Properties of surface-based cohesive behavior

Property	Value	Property	Value	Property	Value
K_n (N/mm^3)	2×10^6	δ_n^{max} (mm)	2.5×10^{-5}	G_n^c (N/mm)	0.06
K_s (N/mm^3)	0.75×10^6	δ_s^{max} (mm)	6.65×10^{-5}	G_s^c (N/mm)	0.06
K_t (N/mm^3)	0.75×10^6	δ_t^{max} (mm)	6.65×10^{-5}	G_t^c (N/mm)	0.06

The most common discrete degradation model is the one proposed by Tan [27], which has been used in many studies on the progressive damage analysis of composite laminates.

3.3 Johnson–Cook flow stress model for aluminum alloy layers

The aluminum alloy layers are modeled as a Johnson–Cook, elastic-plastic material. The Johnson–Cook model, presented by Johnson and Cook [28], is appropriate for modeling high-rate impacts involving metals. In this study, its material parameters are listed in Table 2.

3.4 Surface-based cohesive behavior of the interlaminar delamination

The surface-based cohesive behavior offers capabilities that are same as cohesive elements that are defined by a

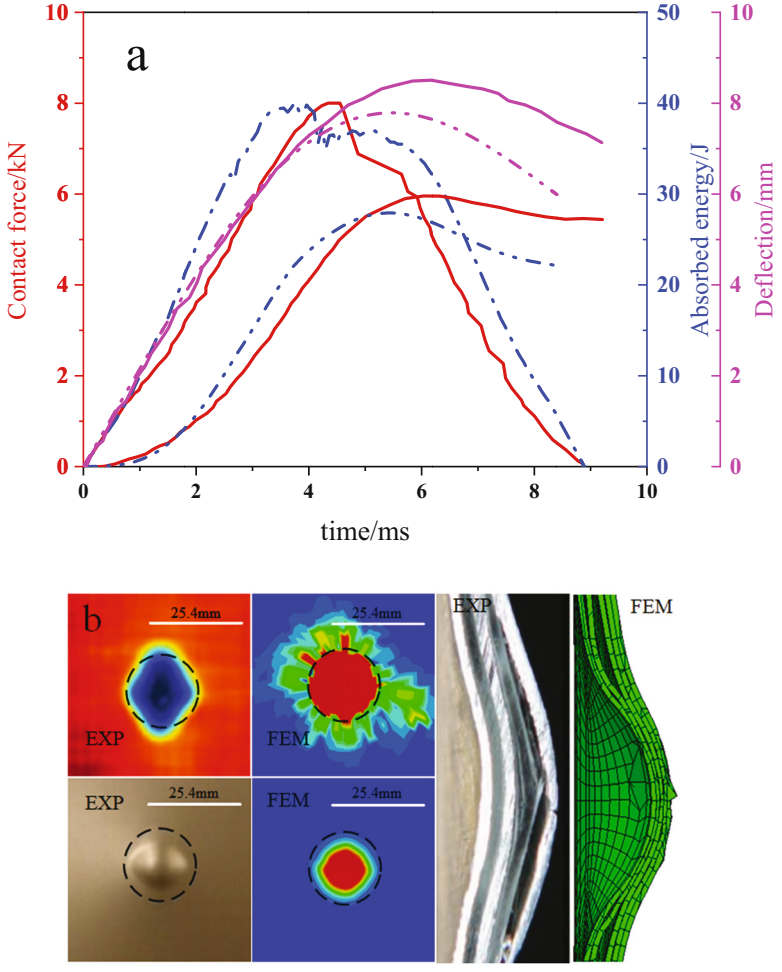

Figure 3: The verification of FEM with the experimental results: (a) impact response history and (b) unrecoverable deformation and interlaminar delamination.

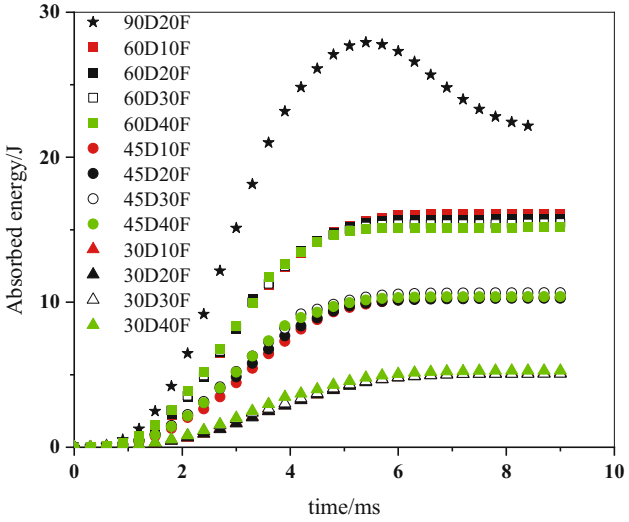

Figure 4: The comparison of history of absorbed energy during the impact process varying in impact angle and contact friction.

traction-separation law. With no limitations of deformation from the cohesive elements, the surface-based cohesive behavior is typically more prone to define and allows simulation in a wider range of cohesive interactions, such as two "sticky" surfaces coming into contact during the analysis. Such numerical implementations are well described in many existing papers. In this study, it is the initiation of damage when maximum nominal stress ratio reaches a value of one. This criterion can be represented as follows:

$$\max\left\{\frac{\langle\sigma_n\rangle}{N_{max}}, \frac{\sigma_s}{S_{max}}, \frac{\sigma_t}{T_{max}}\right\} = 1, \tag{7}$$

where σ_n, σ_s, and σ_t is the instantaneous nominal stress in the pure normal and the first shear and the second shear directions, respectively. While N_{max}, S_{max}, and T_{max} represent the peak values of the nominal stress, when the deformation is either purely normal to the interface or purely in the first or second shear direction, respectively. The Benzeggagh and Kenane (B-K) delamination criterion along with mixed-mode fracture energy laws, which are used to model the initiation and evolution of the damage in delamination [29]. The corresponding properties are shown in Table 3.

4 Results and discussion

With the help of the FEM model, the impact history of curves and damage evolution can be obtained simultaneously so as to reveal the damage mechanism of GLARE.

4.1 Verification of accuracy for FEM

As shown in Figure 3, under an incident energy of 30 J, the simulative results of impact response history are in

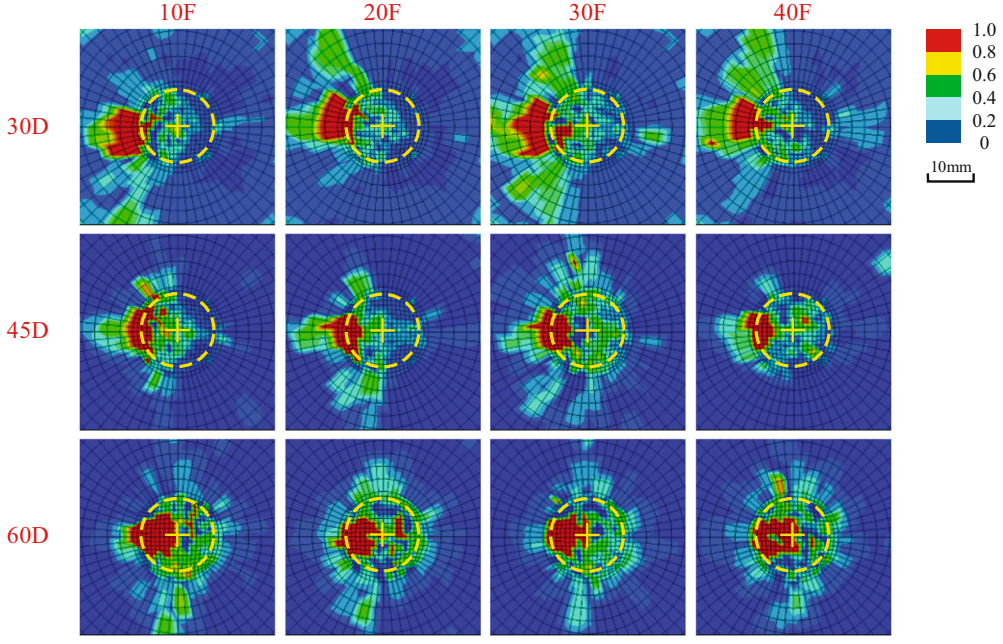

Figure 5: The comparison of interlaminar-delamination between aluminum and GFRP layers after the impact process varying in impact angle and contact friction.

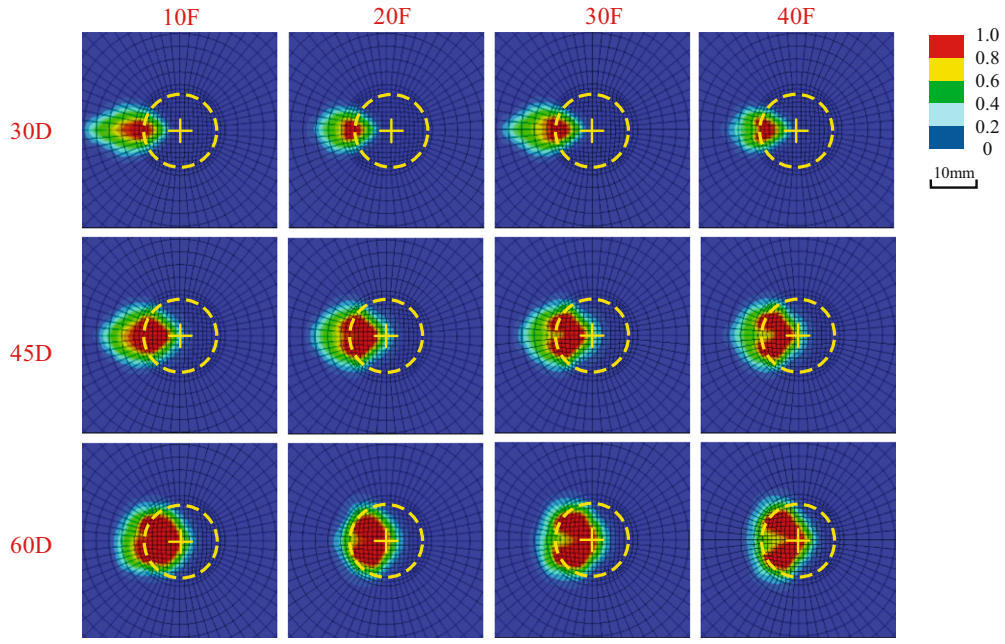

Figure 6: The comparison of failure contour of the aluminum layer after the impact process varying in impact angle and contact friction.

good agreement with the experimental results. The relative error of the peak value is tiny, within the range of 5%. In addition, in terms of interface delamination and permanent deformation pictured in Figure 3, the results of our simulation are in accordance with the experiment results from the literature. Hence, the FEM is reliable for deeper research on the effect of the parameters in the impact events of the GLARE 5 panels on their impact resistance property.

4.2 Comparison of damage history of absorbed energy

Figure 4 compares the absorbed energy history of various impact conditions varying in the impact angle and friction between the impactor and GLARE under the same incident energy of 30 J. The simulative cases are named based on the information on the angle of impact vector direction to the panel and the friction coefficient between the impactor and GLARE. For instance, the case named 60D20F means 60 degrees of impact angle and 0.2 friction coefficient. The results indicate that the ultimate value of absorbed energy is primarily affected by the impact angle rather than the contact friction coefficient. In other words, the absorption of impact kinetic energy is hardly changed by changing the coefficient of friction.

4.3 Comparison of damage behaviors of GLARE 5 subjected LVI varying in angle and friction coefficient

4.3.1 Damage of interlaminar delamination

The interlamination-delamination contour pictures of GLARE 5 between the aluminum and GFRP layer are compared in Figure 5, in which the yellow circles with the diameter of the

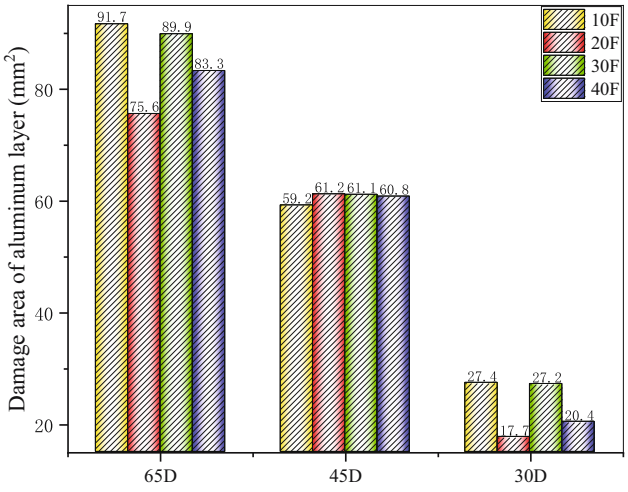

Figure 7: The comparison of damaged area of the aluminum layer after the impact process varying in impact angle and contact friction.

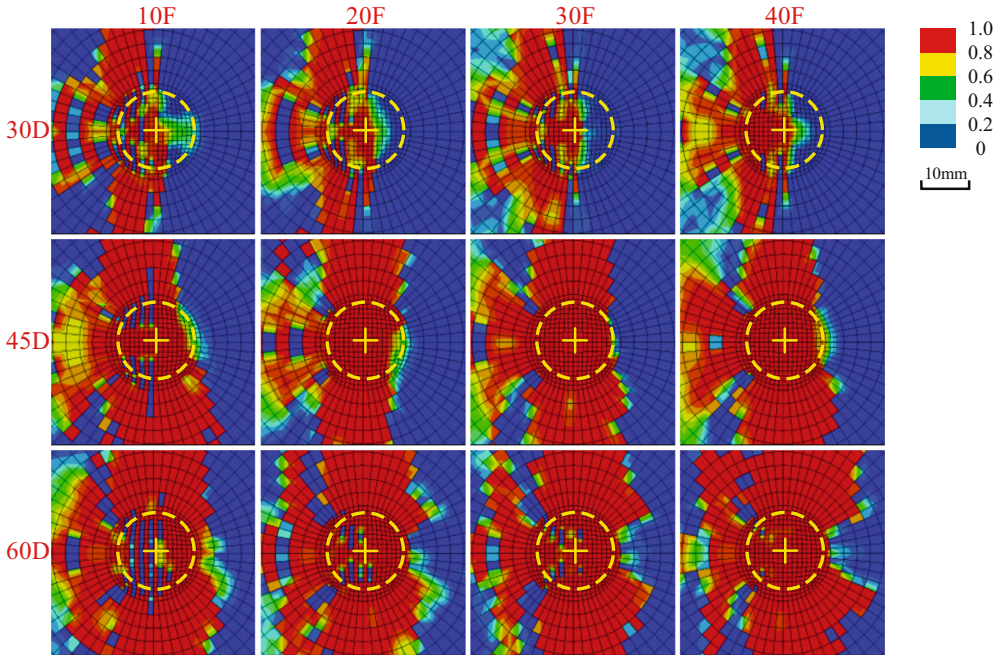

Figure 8: The comparison of tensile damage of the fibers of the GFRP layer after the impact process varying in impact angle and contact friction.

impactor top mark the impactor nose region at the beginning of the LVI events. In general, the damaged area with high damage degree and its distance from the impact point increases with the growth of the impact angle. When the impact angle is 30 degrees, the interlamination-delamination damaged area with low damage degree is wide and located at the side of velocity reversal along the plane. Moreover, as for the friction coefficient between the impactor and the GLARE 5, seeing the figure, a small value of incident energy leads to a wider range of area with damage, especially for the low damage degree.

4.3.2 Damage to aluminum layers

The damage degrees of aluminum layers based on the Johnson–Cook criterion for various impact conditions are discussed and compared in Figure 6. First, on the whole, the damaged area of aluminum layers is concentrated around the impactor nose region. Further, with the increase in the impact angle, as shown in Figure 7, the damaged area of aluminum layers with a high degree rises sharply. However, there is a declining area with a low damage degree.

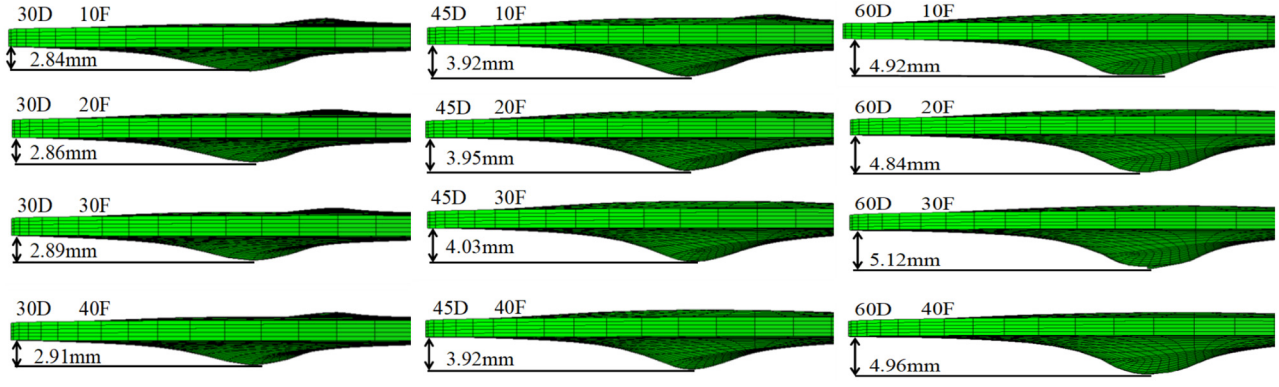

Figure 9: The comparison of unrecoverable deformation of the GFRP layer after the impact process varying in impact angle and contact friction.

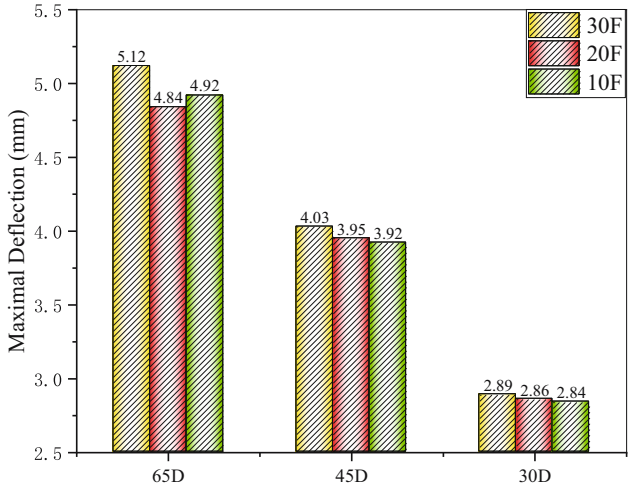

Figure 10: The comparison of peak value of the unrecoverable deformation of the GFRP layer after the impact process varying in impact angle and contact friction.

4.3.3 Damage of GFRP layers

The fiber tensile broken damage of the GFRP layer under different impact angles and friction is pictured and compared in Figure 8. As the impact angle is 30 degrees, there is a small area of damage region mainly located at one-half part of the panel. However, when the incident energy comes up to 60 degrees, in addition, the damaged area around the impactor nose region climbs dramatically. In terms of friction, a higher value leads to a wider failure region.

4.3.4 Comparison of permanent deformation after LVI

As seen in Figures 9 and 10, in general, all unrecoverable deformation of the panels after LVI loading are bell shaped. In addition, there is an offset distance from the impact point to the peak point of the bell-shaped deformation. As for the influence factor of friction, it barely affects the degree of unrecoverable deformation under three different incident energies, which means that the integral deformation of the GLARE panels is determined by kinetic energy at the normal vector to the plane.

5 Conclusion

The effect of the impact angle and contact friction of the GLARE subjected to LVI loading on the impact response history and the failure mode is investigated via numerical simulations. After comparing the unrecoverable deformation and failure contour among the cases varying in the impact angle and contact friction of the GLARE, the summary can be drawn as follows: (1) A methodology in FEM for the GLARE subjected to LVI loading is presented with proper parameters; (2) The oblique LVI loading can lead to a damage mode, offsetting the impact point along the vector of the incident energy; (3) The normal impact kinetic energy affects more on the permanent damage of GLARE than the tangential impact kinetic energy; (4)The tensile damage of the fibers of GFRP layers is more sensitive to the contact friction.

Acknowledgements: This work was supported by Foundation of Jiangxi Province of China Educational Committee (grant number GJJ211910, GJJ190948, GJJ180956, GJJ201907).

Conflict of interest: We declare that we do not have any commercial or associative interest that represents a conflict of interest in connection with the work submitted.

References

[1] Xu LY, Lu JR, Li KM, Hu J. Experimental study of CFRP laser surface modification and bonding characteristics of CFRP/Al6061 heterogeneous joints. Compos Struct. 2022;283:115030.
[2] Mostofinejad D, Moghaddas A. Bond efficiency of EBR and EBROG methods in different flexural failure mechanisms of FRP strengthened RC beams. Constr Build Mater. 2014;54:605–14.
[3] Zhang JF, Chen Q, Shi ZH, Teng JG, Zhou LM. Investigation on a novel bolted joint scheme for foam inserted top-hat stiffened composite plates. Mater Des. 2016;93:448–57.
[4] Zhang JG, Huang Y, Ma XY, Wen XL, Rao J, Dou YK, et al. Effects of layup parameters and interference value on the performance of CFRP–metal interference fit joints. Sci Eng Compos Mater. 2022;29(1):151–64.
[5] Zhu SQ, Chai GB. Low-velocity impact response of fibre–metal laminates–Experimental and finite element analysis. Compos Sci Technol. 2012;72(15):1793–802.
[6] Bunea M, Cîrciumaru A, Buciumeanu M, Bîrsan IG, Silva FS. Low velocity impact response of fabric reinforced hybrid composites with stratified filled epoxy matrix. Compos Sci Technol. 2019;169:242–8.
[7] Wan Y, Diao CY, Yang B, Zhang L, Chen SS. GF/epoxy laminates embedded with wire nets: A way to improve the low-velocity impact resistance and energy absorption ability. Compos Struct. 2018;202:818–35.
[8] Wan Y, Yao J, Li H, Huang YH, You PY, Xu YC, et al. Experimental studies of low-velocity impact behavior on hybrid metal wire net/woven carbon-fiber reinforced composite laminates. Compos Commun. 2022;32:101185.
[9] Wan Y, Yang B, Jin PC, Zheng ZQ, Huang YH. Impact and compression-after-impact behavior of sandwich panel comprised of foam core and wire nets/glass fiber reinforced

epoxy hybrid facesheets. J Sandw Struct Mater. 2021;23(6):2614–37.
[10] Yang B, Wang ZQ, Zhou LM, Zhang JF, Tong LL, Liang WY. Study on the low-velocity impact response and CAI behavior of foam-filled sandwich panels with hybrid facesheet. Compos Struct. 2015;132:1129–40.
[11] Song ZG, Zhang LW, Liew KM. Dynamic responses of CNT reinforced composite plates subjected to impact loading. Compos Part B-Eng. 2016;99:154–61.
[12] Gu GX, Takaffoli M, Hsieh AJ, Buehler MJ. Biomimetic additive manufactured polymer composites for improved impact resistance. Extreme Mech Lett. 2016;9:317–23.
[13] Rafiq A, Merah N, Boukhili R, Al-Qadhi M. Impact resistance of hybrid glass fiber reinforced epoxy/nanoclay composite. Polym Test. 2017;57:1–11.
[14] Vlot A. Impact properties of fibre metal laminates. Compos Eng. 1993;3(10):911–27.
[15] Sadighi M, Alderliesten C, Benedictus R. Impact resistance of fiber-metal laminates: A review. Int J Impact Eng. 2012;49:77–90.
[16] Yu Y, Zhao DC, Feng GL, Geng DX, Guo HS. Energy evolution and acoustic emission characteristics of uniaxial compression failure of anchored layered sandstone. Front Earth Sc-Switz. 2022;10:112.
[17] Guo HS, Chen L, Zhu JY, Sun QC, Xiao YX. Application of borehole camera technology in the identification of an instantaneous strain-structural-plane slip rockburst. B Eng Geol Env. 2022;81(5):1–13.
[18] Zhang HN, Chen CX, Zheng Y, Yu QQ, Zhang W. Centrifuge modeling of layered rock slopes susceptible to block-flexure toppling failure. B Eng Geol Env. 2020;79(7):3815–31.
[19] Zhang JH, Li J, Yao YS, Zheng JL, Gu F. Geometric anisotropy modeling and shear behavior evaluation of graded crushed rocks. Constr Build Mater. 2018;183:346–55.
[20] Li LJ, Sun LY, Wang TK, Kang N, Cao W. Repeated low-velocity impact response and damage mechanism of glass fiber aluminium laminates. Aerosp Sci Technol. 2019;84:995–1010.
[21] Bienias J, Jakubczak P, Dadej K. Low-velocity impact resistance of aluminium glass laminates–experimental and numerical investigation. Compos Struct. 2016;152:339–48.
[22] Seyed Yaghoubi A, Liu Y, Liaw B. Low-velocity impact on GLARE 5 fiber-metal laminates: influences of specimen thickness and impactor mass. J Aerosp Eng. 2012;25(3):409–20.
[23] Morinière FD, Alderliesten RC, Tooski MY, Benedictus R. Damage evolution in GLARE fibre-metal laminate under repeated low-velocity impact tests. Cent Eur J Eng. 2012;2(4):603–11.
[24] Soltani P, Keikhosravy M, Oskouei RH, Soutis C. Studying the tensile behaviour of GLARE laminates: a finite element modelling approach. Appl Compos Mater. 2011;18(4):271–82.
[25] Al-Azzawi ASM, Kawashita LF, Featherston CA. Buckling and postbuckling behaviour of Glare laminates containing splices and doublers. Part 2: Numerical modelling. Compos Struct. 2017;176:1170–87.
[26] Hashin Z. Failure criteria for unidirectional fiber composites. J Appl Mech. 1980;47(2):329–34.
[27] Tan SC. A progressive failure model for composite laminates containing opening. J Compos. 1991;25(5):556–77.
[28] Johnson GR, Cook WH. A constitutive model and data for metals subjected to large strains, high strain rates and high temperatures. In: Proceedings of the seventh international sympo-sium on ballistics. The Hague, Netherland: 1983. p. 541–7.
[29] Benzeggagh ML, Kenane M. Measurement of mixed-mode delamination fracture toughness of unidirectional glass/epoxy composites with mixed-mode bending apparatus. Compos Sci Technol. 1996;56(4):439–49.